MINOS RESULTS, PROGRESS AND FUTURE PROSPECTS

TOBIAS M. RAUFER, FOR THE MINOS COLLABORATION
University of Oxford, Sub-dept. of Particle Physics
Denys Wilkinson Building, Keble Road
Oxford OX1 3RH. United Kingdom

The MINOS long baseline experiment has been collecting neutrino beam data since March 2005 and has accumulated 3×10^{20} protons-on-target (POT) to date. MINOS uses Fermilab's NuMI neutrino beam which is measured by two steel-scintillator tracking calorimeters, one at Fermilab and the other 735 km downstream, in northern Minnesota. By observing the oscillatory structure in the neutrino energy spectrum, MINOS can precisely measure the neutrino oscillation parameters in the atmospheric sector. From analysis of the first year of data, corresponding to 1.27×10^{20} POT, these parameters were determined to be $|\Delta m^2_{32}| = 2.74^{+0.44}_{-0.26} \times 10^{-3}\,\mathrm{eV}^2/c^4$ and $\sin^2(2\theta_{23}) > 0.87$ (68% C.L.). MINOS is able to measure the neutrino velocity by comparing the arrival times of the neutrino beam in its two detectors. Using a total of 473 Far Detector events, $(v - c)/c = (5.1 \pm 2.9) \times 10^{-5}$ (68% C.L.) was measured. In addition, we report recent progress in the analysis of neutral current events and give an outline of experimental goals for the future.

1 Introduction

It is now well established that neutrinos have non-zero masses and that neutrinos mix. Their weak interaction eigenstates (or "flavour" eigenstates) ν_α are related to their mass eigenstates ν_i by a unitary transformation U:

$$|\nu_\alpha\rangle = \sum_i U^*_{\alpha i}|\nu_i\rangle \tag{1}$$

U is called the PMNS [1,2] matrix. Neutrinos are created and detected by weak interaction processes but their propagation in free space is described by their mass eigenstates, causing relative phases to change. This leads to the phenomenon of neutrino oscillations.

MINOS is a long baseline neutrino oscillation search based at FNAL. The neutrino beam created in the NuMI beamline is sampled in two locations, ∼1 km from the beam production

Correspondence: `t.raufer1@physics.ox.ac.uk`

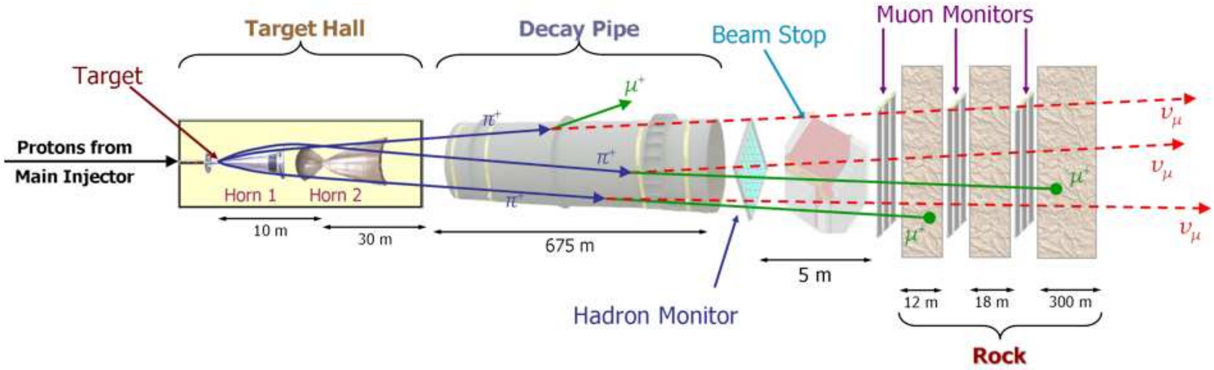

Figure 1: The NuMI beamline components. Positively charged mesons produced in the target are focused by two magnetic horns and subsequently decay in a 675 m-long evacuated volume producing predominantly ν_μ. The remaining hadrons are stopped in a beam absorber at the end of the decay pipe.

target underground at Fermilab, and again 735 km downstream in the Soudan Underground Laboratory, in Minnesota.

Using this setup, MINOS measures the oscillation parameters $|\Delta m^2_{32}|$and $\sin^2(2\theta_{23})$to world leading precision. In addition, MINOS searches for sub-dominant $\nu_\mu \to \nu_e$ oscillations, oscillations into sterile neutrinos, and $\nu \to \overline{\nu}$ transitions. The MINOS Far Detector can also be used to detect neutrinos created in the atmosphere. [3,4]

2 Experimental setup

2.1 The NuMI beamline

A schematic of the NuMI neutrino beamline is shown in Figure 1. NuMI uses protons with a momentum of 120 GeV extracted from Fermilab's Main Injector accelerator. They impinge a 95.4 cm long segmented graphite target producing secondary particles, mainly π and K mesons. The positively charged mesons are focused using a system of two pulsed, parabolic magnetic focusing elements, called "horns". The secondaries subsequently decay in a 675 m long, 2 m diameter evacuated decay volume producing neutrinos.

Hadrons reaching the end of the decay volume without decaying are stopped in an beam absorber following the decay pipe. The beam absorber consists of a water-cooled aluminium core surrounded by a layer of steel blocks and an outer layer of concrete. The remaining muons from the meson decays are stopped in the $\sim$300 m of rock that separate the MINOS Near Detector hall from the beam absorber.

The target position relative to the first horn and the horn current are variable. For most of the collection of data used in the oscillations analysis presented here, the target was inserted 50.4 cm into the first horn to maximize neutrino production in the 1-3 GeV energy range. The data described here were recorded in this position, between May 2005 and February 2006, and correspond to a total of 1.27×10^{20} POT. The charged current (CC) neutrino event yields at the ND are predicted to be 92.9% ν_μ, 5.8% $\overline{\nu}_\mu$, 1.2% ν_e and 0.1% $\overline{\nu}_e$.

2.2 The MINOS detectors

The MINOS detectors are designed to be as similar as possible while operating in very different conditions. They are steel-scintillator sampling calorimeters, magnetized to $\sim$1.3 T allowing to measure particle momentum using track curvature as well as range. The scintillator planes are divided into 4.1 cm wide strips rotated by 90° on subsequent planes to enable 3-dimensional event reconstruction. The scintillator light is captured by embedded wavelength shifting (WLS) fibres and transported to the edge of the detectors, where the optical signal is converted using Hamamatsu M64 [5] (Near Detector) and M16 [6] (Far Detector) photomultiplier tubes.

Below 10 GeV, the hadronic energy resolution was measured to be $56\%/\sqrt{E[\text{GeV}]} \oplus 2\%$ and the EM resolution was measured to be $21.4\%/\sqrt{E[\text{GeV}]} \oplus 4.1\%/E[\text{GeV}]$. [7] The muon energy resolution $\Delta E_\mu/E_\mu$ varies smoothly from 6% for E_μ above 1 GeV where most tracks are contained and measured by range, to 13% at high energies, where the curvature measurement is primarily used.

3 Monte Carlo tuning

MINOS took data with 6 beam configurations obtained by varying the target position and the current in the focusing horns. The Monte Carlo simulations of neutrino fluxes strongly depend on the underlying models of hadron production in the target, which are presently poorly constrained at MINOS energies. The nominal simulations, based on `FLUKA05`, yielded energy spectra which did not match the high-statistics data in the Near Detector. A better agreement was achieved by smoothly adjusting the p_z and p_T of hadrons (mostly pions) produced off the graphite target. The resulting spectra, which describe the data much more closely than the nominal simulations, are shown in Figure 2.

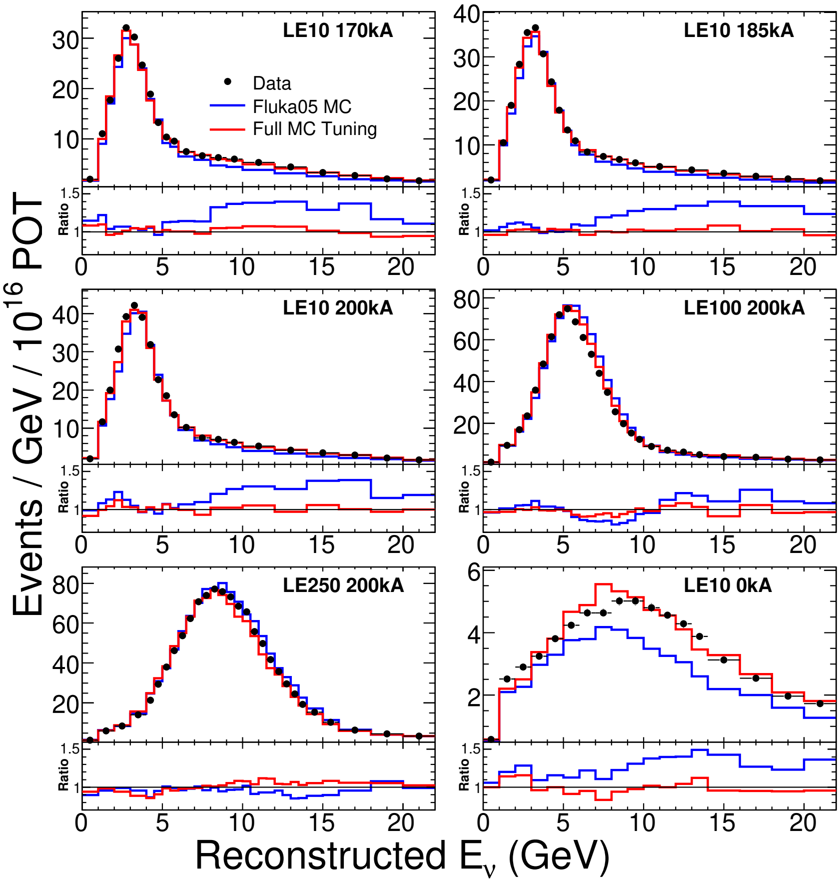

Figure 2: Data and Monte Carlo energy spectra and their ratios are shown for six deferent beam configurations. The blue line corresponds to the untuned, the red line to the tuned hadron production model. The tuning significantly improves data/MC agreement in all cases.

4 ν_μ disappearance analysis

4.1 Event selection and extrapolation

In the Far Detector (FD), the signal from eight scintillator strips is read out by the same PMT pixel. Therefore, the initial step in the reconstruction of the FD data is the removal of the eightfold hit-to-strip ambiguity using information from both strip ends. In the ND, timing and spatial information is first used to separate individual neutrino interactions from the same spill. Subsequent reconstruction is done in the same way in both detectors. Tracks are found and fitted, and showers are reconstructed to be combined to events. For ν_μ CC events, the total reconstructed event energy is obtained by summing the muon energy and the visible energy of the hadronic system. To prevent human biases when assessing the oscillation analysis results, a blinding mechanism was applied to the FD data set. This procedure hid a substantial fraction of the FD events with the precise fraction and energy spectrum of the hidden sample unknown. Events are pre-selected in both detectors, by requiring total reconstructed energy below 30 GeV and a negatively charged track. The track vertex must be within a fiducial volume such that cosmic rays are rejected and the hadronic energy of the event is contained within the volume of the detector. The pre-selected ν_μ event sample is predominantly CC with a 8.6% neutral current (NC) event background estimated from Monte Carlo (MC) simulations. The fiducial mass of the FD and ND is 72.9% and 4.5% of the total detector mass respectively.

A particle identification parameter (PID) incorporating probability density functions for the event length, the fraction of energy contained in the track and the average track pulse height per plane provides separation of ν_μ CC and NC events. The PID is shown in Figure 3 for ND and FD data overlaid with simulations of NC and CC events. Events with PID above -0.2 (FD) and -0.1 (ND) are selected as being predominantly CC in origin. These values were optimized for both detectors such that the resulting purity of each sample is about 98%. The efficiencies for selecting ν_μ CC events in the fiducial volume with energy below 30 GeV are 74% (FD) and 67% (ND).

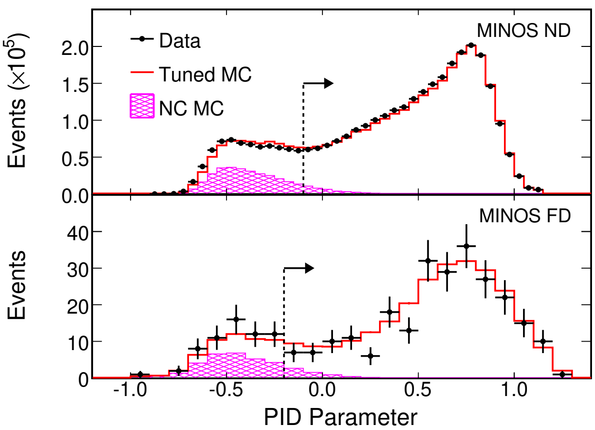

Figure 3: Data and tuned MC predictions for the PID variable in the ND (top) and FD (bottom). The arrows depict the positions of the selection cuts. The FD MC distribution for CC events uses the best fit parameters discussed in the text.

The measurement of the energy spectrum at the ND is used to predict the unoscillated spectrum at the FD. Fits to the ND data yield tuning parameters for the predicted neutrino flux. These fits are based on parameterisations of the secondary pion production at the NuMI target as a function of x_F and p_T as described in Section 3. The FD prediction must also take into account the ND and FD spectral differences that are present, even in the absence of oscillations, due to pion decay kinematics and beamline geometry. This is achieved using the *Beam Matrix* method. It utilizes the beam simulation to derive a transfer matrix that relates the neutrinos in the two detectors via their parent hadrons. The ND reconstructed event energy spectrum is translated into a flux by first correcting for the simulated ND acceptance and then dividing by the calculated cross-sections for each energy bin. This flux is multiplied by the transfer matrix to yield the predicted, unoscillated FD flux. After an inverse correction for cross-section and FD acceptance, the predicted FD visible energy spectrum is obtained. The oscillation hypotheses are then tested relative to this prediction. A distinct extrapolation method, referred to as *ND Fit* was also applied to the data, yielding similar results.

In total, 215 events are observed below 30 GeV compared to 336.0±18.3(stat.)±14.4(syst.) events expected in the absence of oscillations. The systematic error is most relevantly due to NC contamination, ND to FD normalization and the hadronic shower energy scale. In the region below 10 GeV, 122 events are observed compared to the expectation of 238.7±15.4±10.7. The observed energy spectrum is shown along with the predicted spectra for both extrapolation methods in Figure 4.

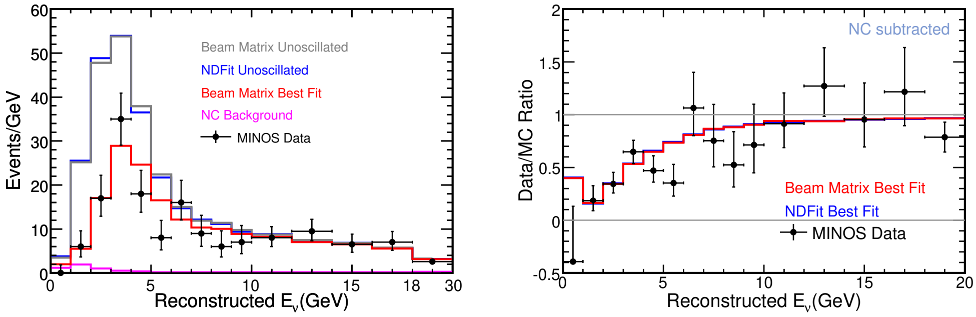

Figure 4: Comparison of the Far Detector spectrum with predictions for no oscillations for both analysis methods and for oscillations with the best fit parameters from the Beam Matrix extrapolation method (left canvas). The estimated NC background is also shown. The last energy bin contains events between 18-30 GeV. The right canvas shows the ratio of data and best fit over the unoscillated predictions.

4.2 Oscillation analysis

Under the assumption that the observed deficit is due to $\nu_\mu \to \nu_\tau$ oscillations, a χ^2 fit is performed to the parameters $|\Delta m^2_{32}|$ and $\sin^2(2\theta_{23})$ using the expression for the ν_μ survival probability:

$$P(\nu_\mu \to \nu_\mu) = 1 - \sin^2(2\theta_{23}) \sin^2\left(\frac{\Delta m^2_{32} L}{4E}\right) \tag{2}$$

where L is the distance from the target, E is the neutrino energy, and $|\Delta m^2_{32}|$ is the atmospheric mass splitting. The fit included the systematic uncertainties mentioned above as nuisance parameters as well as the small contribution from selected ν_τ events produced in the oscillation process. The resulting 68% and 90% confidence intervals are shown in Figure 5 as determined from $\Delta\chi^2$=2.3 and 4.6, respectively. The best fit parameter values are:

$$|\Delta m^2_{32}| = (2.74\,^{+0.44}_{-0.26}) \times 10^{-3}\,\mathrm{eV}^2/c^4 \tag{3}$$

and

$$\sin^2(2\theta_{23}) > 0.87 \tag{4}$$

at 68% C.L. with a fit probability of 8.9%. At 90% C.L.$(2.31 < |\Delta m^2_{32}| < 3.43) \times 10^{-3}\,\mathrm{eV}^2/c^4$, and $\sin^2(2\theta_{23}) > 0.78$. The data and best fit MC are shown in Figure 4.

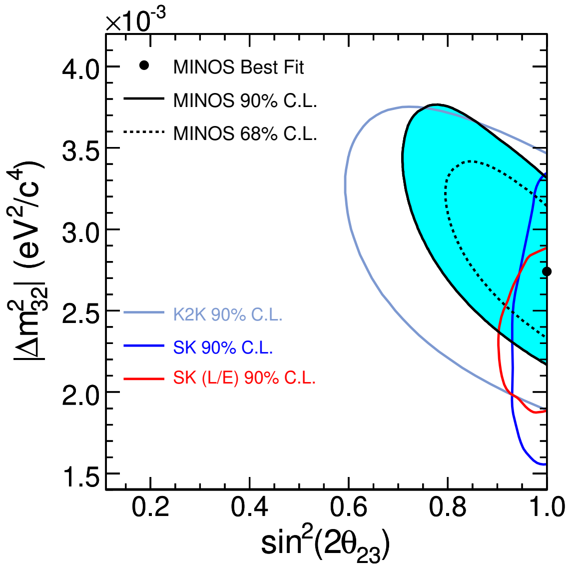

Figure 5: Confidence intervals for the fit using the Beam Matrix method including systematic errors. Also shown are the contours from the previous highest precision experiments. [8,9,10]

If the fit is not constrained to be within the physical region, the best fit is at $|\Delta m^2_{32}|$=$2.72 \times 10^{-3}\,\mathrm{eV}^2/c^4$ and $\sin^2(2\theta_{23})$= 1.01, with a decrease in χ^2 of 0.2.

It is expected that the systematic uncertainties will be reduced with additional data. More details of this analysis are available in [11]. An update on this result using 2.58×10^{20} POT is expected during the Summer 2007.

5 Neutrino time-of-flight analysis

MINOS uses GPS synchronized clocks to timestamp neutrino interactions in both detectors. This enables the measurement of the neutrino time-of-flight over a distance of 734 km and thus the determination of the neutrino velocity. Similar terrestrial experiments performed in the past used much shorter baselines of ~ 500 m and higher beam energies (> 30 GeV).

The time of each PMT hit is recorded by the detector's clock to a precision of 18.8 ns in the Near Detector and 1.6 ns in the Far Detector. The time of the earliest hit of each event is taken to be the time of the neutrino interaction. The interaction times t_1 and t_2 in the two detectors are corrected for known offsets and delays, which were determined using test stand measurements. In addition, the time of the beam extraction signal is subtracted from both times. The beam extraction signal has a fixed relation to the arrival of neutrinos in the MINOS detectors. All times are therefore measured relative to this reference.

The NuMI beam pulse is not instantaneous, but has a duration of $9.7\,\mu s$ with a five-batch or six-batch intensity profile depending on the accelerator running mode. The Near Detectors measures this time-intensity profile with neutrino interactions to high precision. The measured time-intensity profile forms a probability density function which is folded with a Gaussian distribution with a width of $\sigma = 150\,ns$ to account for the uncorrelated jitter of the two GPS clocks. The resulting distribution $P(t)$ describes the predicted arrival time distribution at the Far Detector (shown as a solid line in Figure 6 for the five- and six-batch modes separately).

For the time-of-flight measurement, 473 neutrino-induced events in the Far Detector were used. The time of each event was compared to the predicted arrival time distribution. The

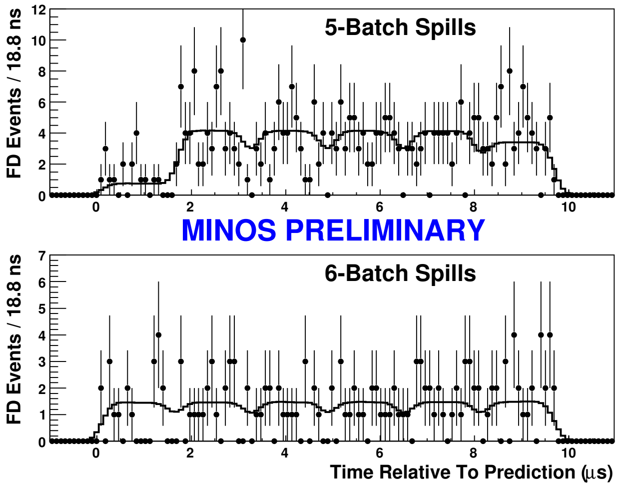

Figure 6: Time distribution of FD events relative to prediction after fitting the time-of-flight. The top plot shows events in 5-batch spills, the bottom 6-batch spills. The solid lines show the normalized prediction curves.

time-of-flight τ was found by maximizing an unbinned log-likelihood function:

$$L = \sum_i \ln P(t_2^i - \tau). \tag{5}$$

The distribution of measured event times together with the predicted distribution for the best fit τ is shown in Figure 6. The time-of-flight of neutrinos was measured to be

$$2449.223 \pm 0.032(\text{stat.}) \pm 0.064(\text{syst.})\ \mu\text{s} \qquad 68\%\ \text{C.L.} \tag{6}$$

Comparing to the MINOS baseline this translates to

$$\frac{(v-c)}{c} = 5.1 \pm 2.9\,(\text{stat.} + \text{sys.}) \times 10^{-5} \qquad 68\%\ \text{C.L.} \tag{7}$$

The systematic error is due to uncertainties on the timing delays and offsets.

6 Progress in Neutral Current analyses

Analyses of neutral current neutrino interactions in MINOS are currently in progress. Neutral current interactions are interesting for several reasons. They form an important background to the $\nu_\mu \to \nu_\tau$ oscillation analysis described in these proceedings and their cross-sections at the energies relevant to MINOS are not very well known. Furthermore, an observed deficit of neutral current events at the Far Detector could be evidence for light sterile neutrinos.

Neutral current interactions are selected using three event quantities: the event length, the number of tracks in the event and the *track extension*. In events where both tracks and showers were found, the track extension measures how much longer a reconstructed track is compared to the hadronic shower it is accompanied by. Distributions of the selection variables in Near Detector data and Monte Carlo are shown in Figure 7 (left canvas).

Using these variables, an energy spectrum of neutral-current-like events was produced. This is shown in the right canvas of Figure 7. The Monte Carlo is shown as a red line with a systematic error band; the background due to wrongly selected charged current events is shown as a blue hatched distribution. Within the estimated systematic errors, due to flux, cross-section and energy scale uncertainties, data and Monte Carlo agree well.

The extrapolation of these Near Detector results to the Far Detector and a fit for oscillations to sterile neutrinos are currently being worked on. Results from this analysis are expected later this year.

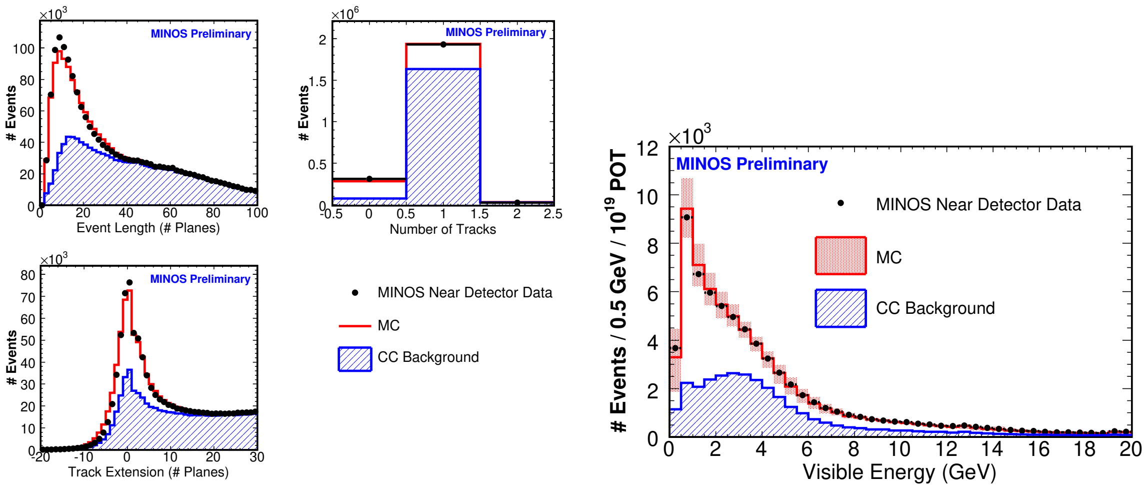

Figure 7: Neutral current event selection variables in the Near Detector (left). The data is shown as black markers, the Monte Carlo in red. The blue distribution shows the charged current background. The right canvas shows the reconstructed energy spectrum for selected neutral current events. The Monte Carlo (red) is shown with systematic errors.

7 Future Prospects

In addition to the analyses reported here, MINOS is pursuing a $\nu_\mu \to \nu_e$ oscillation analysis in order to measure or constrain the as yet unknown mixing angle θ_{13}. With its expected final statistics, MINOS will potentially be able to improve on the current best limit from the CHOOZ [12] experiment.

Other areas of interest include appearance and disappearance measurements of anti-neutrinos in the Far Detector as well as several non-oscillation analyses using the large number of neutrino interactions in the Near Detector.

Acknowledgments

This work was supported by the US DOE; the UK PPARC; the US NSF; the State and University of Minnesota; the University of Athens, Greece and Brazil's FAPESP and CNPq. We are grateful to the Minnesota Department of Natural Resources, the crew of the Soudan Underground Laboratory, and the staff of Fermilab for their contributions to this effort.

References

1. B. Pontecorvo, *Sov. Phys. JETP* **7**, 172 (1958).
2. Z. Maki and M. Nakagawa and S. Sakata, *Progr. Theor. Phys.* **28**, 870 (1962).
3. P. Adamson *et al.* [MINOS Collaboration], *Phys. Rev.* D **73**, 072002 (2006).
4. P. Adamson *et al.* [MINOS Collaboration], *Phys. Rev.* D **75**, 092003 (2007).
5. N. Tagg *et al.*, *Nucl. Instrum. Methods* A **539**, 668 (2005).
6. K. Lang *et al.*, *Nucl. Instrum. Methods* A **545**, 852 (2005).
7. P. Adamson *et al.*,*Nucl. Instrum. Methods* A **556**, 119 (2006).
8. Y. Ashie *et al.*, *Phys. Rev. Lett.* **93**, 101801 (2004).
9. Y. Ashie *et al.*, *Phys. Rev.* D **71**, 112005 (2005).
10. E. Aliu *et al.*, *Phys. Rev. Lett.* **94**, 081802 (2005).
11. D.G. Michael *et al.* [MINOS Collaboration], *Phys. Rev. Lett.* **97**, 191801 (2006).
12. M. Apollonio *et al.*, *Phys. Lett. B* **466**, 415 (1999).